






Ultrafast relaxation of acoustic and optical phonons in a topological nodal-line semimetal ZrSiS

Yangyang Liu ¹, Gyanendra Dhakal¹, Anup Pradhan Sakhya¹, John E. Beetar^{1,5}, Firoza Kabir¹, Sabin Regmi ¹, Dariusz Kaczorowski ², Michael Chini ^{1,3}, Benjamin M. Fregoso ⁴✉ & Madhab Neupane¹✉

Recently, nodal line semimetals based on ZrSiS-family have garnered massive research interests contributing numerous experimental and theoretical works. Despite being the most studied nodal-line semimetal, a clear understanding of the transient state relaxation dynamics and the underlying mechanism in ZrSiS is lacking. Using time- and angle-resolved photoemission spectroscopy, we study the ultrafast relaxation dynamics in ZrSiS and reveal a unique relaxation in the bulk nodal-line state which is well-captured by a simple model based on optical and acoustic phonon cooling. Our model predicts linear decay processes for both optical and acoustic phonon relaxations with optical cooling dominant at higher temperatures. Our results reveal different decay mechanisms for the bulk and surface states and pave a way to understand the mechanism of conduction in this material.

¹Department of Physics, University of Central Florida, Orlando, FL 32816, USA. ²Institute of Low Temperature and Structure Research, Polish Academy of Sciences, ul. Okólna 2, 50-422 Wrocław, Poland. ³CREOL, the College of Optics and Photonics, University of Central Florida, Orlando, FL 32816, USA. ⁴Department of Physics, Kent State University, Kent, OH 44242, USA. ⁵Present address: Department of Chemistry, UC Berkeley, Berkeley, CA, USA. ✉email: benjamin.fregoso@gmail.com; Madhab.Neupane@ucf.edu

In topological semimetals, valence and conduction bands cross each other in momentum space with crossings protected by crystal and/or time-reversal symmetries resulting in intriguing electronic and transport properties^{1–5}. Topological Dirac and Weyl semimetals are characterized by band crossings between bulk conduction and valence bands at discrete k -points in the Brillouin zone^{6,7}, whereas topological nodal line semimetals (TNSMs) are characterized by the band-crossings along a line or a ring^{8–14}. TNSMs have been theoretically^{8,15–19} and experimentally explored in diverse material systems^{9,10,20–24}. The extension of band crossings to a line or a ring in TNSMs leads to an increase in the density of states of carriers in these bands, thus providing greater carrier density with which the photons can interact²⁵. The increased density of Dirac fermions in TNSMs are favorable for the presence of electron correlation effects²⁶.

ZrXY family of materials where $X = \text{Si, Sn, Ge}$ and $Y = \text{S, Se, Te}$ are among the most studied TNSMs due to their high crystal quality and flexibility of the chemical composition^{9,10,27–38}. Among the ZrXY, ZrSiS is especially interesting because it possesses linearly dispersing bands extending up to 2 eV, which are free from interference from trivial bands making this material an excellent prospect for studying Dirac physics²⁷. Even though several experimental studies have been reported on ZrSiS such as angle-resolved photoemission spectroscopy (ARPES)^{9,10,30,31,37}, high-field magnetotransport measurements^{39,40}, scanning tunneling microscopy⁴¹, frequency-independent optical conductivity⁴², high carrier mobility^{40,43}, the experimental and theoretical description of the effect of phonon scattering in electron cooling processes have not been studied so far. Using time-resolved ARPES (tr-ARPES), it has been observed that the electronic correlations in ZrSiSe can be reduced by optical excitation of high-energy electron-hole pairs, which screens the Coulomb interaction thus leading to renormalization of the Dirac quasiparticles¹⁴. A recent study on ultrafast optical response of ZrSiS and ZrSiSe in the near-infrared using transient reflectivity reveal two responses with different time scales. The first decays after hundreds of femtoseconds whereas the other lasts for nanoseconds which were explained as a sudden change of the electronic properties such as an increase in the electronic screening or the reduction of the plasma frequency followed by an increase of the Drude scattering rate²⁵.

Although some ultrafast optical studies have been reported^{25,44} which are based on transient reflectivity and provide some information about the relaxation dynamics, a clear understanding of how the excited electrons relax and what is the physical process by which it occurs is yet to be understood. Electron cooling can be probed by using time-resolved pump-probe spectroscopy and the relaxation dynamics can be used to shed light on the electron-electron interaction, electron-phonon interaction etc. Ultrafast relaxation dynamic studies are essential in studying materials that have been excited away from equilibrium which helps in understanding fast processes and manipulating their electronic and optical properties⁴⁵.

Here, we report the ultrafast relaxation of optical and acoustic phonons in a ZrSiS. We observe slow relaxation decay of bulk nodal line in contrast to Dirac-like surface state. Our theoretical modeling based on optical and acoustic phonon cooling matches well with the observed experimental findings, which reveals that optical phonon cooling is always dominant at higher temperatures, which results in a fast relaxation decay, whereas a sharp crossover from the optical phonon cooling to acoustic phonon cooling takes place at lower temperature resulting in slower relaxation decay. Concomitantly, both relaxation processes adhere linear decay. This work could provide a simple approach to understand the relaxation dynamics in other nodal-line semimetals.

Results

Electronic properties of equilibrium state of ZrSiS. ZrSiS crystallizes in the tetragonal crystal structure with space group $P4/nmm$ and is presented in Fig. 1b. The Fermi surface measured using a photon energy of 30 eV is shown in Fig. 1c. A diamond-shaped Fermi pocket around the Γ point and an elliptical pocket around the X point of the Brillouin zone are observed. In the leftmost panel of Fig. 1d, we present the Fermi surface obtained using our tr-ARPES set-up and the right panels in Fig. 1d show the constant energy contours at various binding energies equal to 280, 650, and 900 meV, respectively. The Fermi surface obtained from tr-ARPES is consistent with the Fermi surface obtained from our synchrotron results as shown in Fig. 1c thus suggesting that extreme ultraviolet (XUV) based tr-ARPES is good enough for the detailed characterization of the ultrafast dynamics in ZrSiS. ZrSiS possesses a bulk nodal-line around the Γ point, which arises from the p_x and p_y orbitals in the Si square net and the nearby Zr-d orbitals¹⁰. The band structure of the material also exhibits Dirac crossing at the X point, which is protected by the nonsymmorphic symmetry of the crystal structure³⁷.

Electronic properties of non-equilibrium state of ZrSiS. In the following, we will focus on discussing the ultrafast dynamics of ZrSiS. A pump pulse with a photon energy of 1.2 eV is used to excite the sample and the transient electronic structure is probed along the Γ - M direction by an ultrashort XUV pulse of 21.8 eV as shown in Fig. 2. Figure 2a, b show the bulk nodal-line state at two different time delays. Figure 2a is measured at a delay of -6.3 ps, which means the probe pulse is 6.3 ps earlier than the pump pulse. The measured linearly dispersing nodal-line bulk bands are consistent with the previous study⁹, and reasonably, no photoexcited states are observed above the Fermi level. When the delay time between the pump and the probe pulse is changed to 0.4 ps, the electrons are excited above the Fermi level by the pump pulse and the transient electronic structure is probed by the ultrashort XUV pulse, which is illustrated in Fig. 2b. For additional measurements at various time delays, see Supplementary Note 1 and Supplementary Fig. 1.

In order to systematically study the ultrafast dynamics of the hot electrons of the nodal-line bulk states, we proceed to analyze the transient electronic distributions. First, the temperature of the hot electrons over the time delay is analyzed by integrating the momentum of the ARPES spectra to get the energy distribution curves (EDCs), and then extracting the electronic temperatures by fitting the EDCs with the Fermi-Dirac distribution as a function of the time delay, which is shown as red dots in Fig. 2c. At negative delays, the electronic temperature stays at around 300 K as the measurement is performed at room temperature. Upon excitation, the electronic temperature suddenly increases to around 1200 K at 0.4 ps, then drops to around 450 K at 6 ps. The structure of the measured transient electronic temperature can be considered as containing three parts: a very sharp increase (0–0.4 ps), a fast decay (0.4–2 ps), and another slow decay (2–6 ps). The transient temperature is fitted with a convolution between a Gaussian pulse and a bi-exponential decay, which is shown as the red line in Fig. 2c. From the fitting curve, the fast and the slow relaxation time constants can be extracted, which are 0.6 and 20 ps, respectively.

With the aim of understanding the transient dynamics of the Dirac-like surface states, we have performed ultrafast pump-probe spectroscopy measurements along the X - M direction as shown in Fig. 3. Figure 3a, b show the ARPES spectra measured at different time delays between the pump and probe pulses. Figure 3a shows the ARPES spectra before the pump pulse excites the electrons and hence no states are observed above the Fermi level. In Fig. 3b, we can

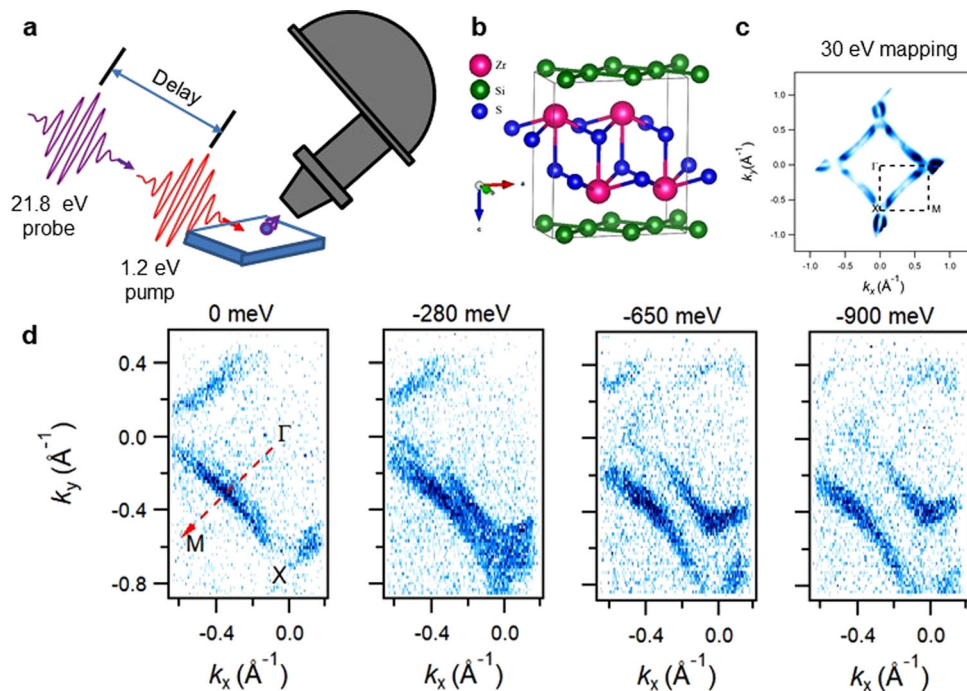


Fig. 1 Angle-resolved photoemission spectroscopy (ARPES) measurements of ZrSiS. **a** Schematic view of pump-probe ARPES set-up. The photon energies of the pump and probe pulse are 1.2 and 21.8 eV, respectively. **b** Tetragonal crystal structure of ZrSiS. **c** Measured Fermi surface map of ZrSiS using a photon energy of 30 eV. It consists of two diamond shaped pockets formed by the crossing of the bulk valence and conduction bands and an additional pocket at the X point formed by the surface state. **d** Fermi surface (leftmost panel) and constant energy contours at various binding energies as noted on top of the contours. The measurements in panel d were performed in our home-built static ARPES system.

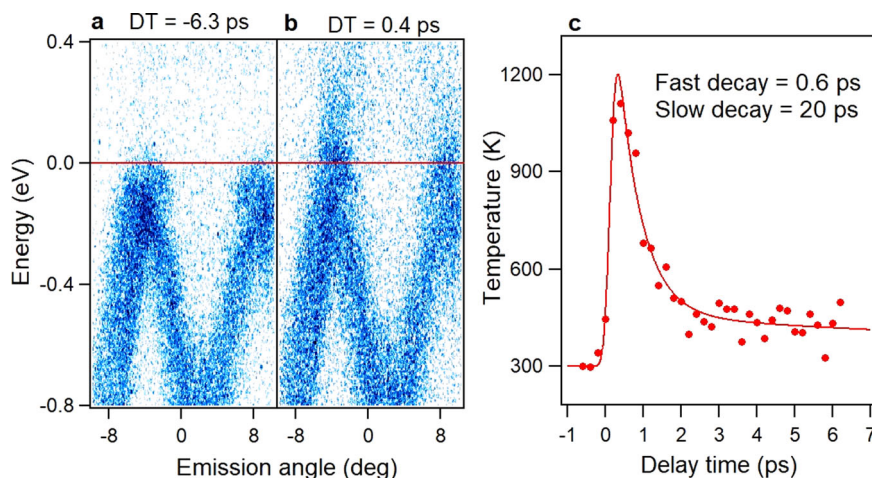


Fig. 2 Time-resolved angle-resolved photoemission spectroscopy measurements of the nodal-line bulk states. Experimental band dispersion measured along the Γ -M direction at delay times of **a** -6.3 ps and **b** 0.4 ps. The states above the Fermi level, i.e., the non-equilibrium states can be observed only when the delay value is positive. **c** The transient electronic temperature as a function of the time delay (red dots) and the corresponding fitting curve (solid line). The fitting function is the convolution between a Gaussian pulse and a bi-exponential decay.

see the upper region of the Dirac cone is populated at a positive time delay of 0.4 ps after photoexcitation. The Dirac point is found to be around 280 meV below the Fermi level, which is consistent with the previous result⁹. To analyze the response of the photo-induced perturbation in this Dirac-like state, we integrated the momentum of the ARPES spectra within the range from -10° to 10° to obtain the experimental EDCs, which was fitted by considering the spectral function as a representation of the Fermi-Dirac distribution function for various time delays to extract the electronic temperatures, see Supplementary Fig. 2 and Supplementary Note 2 for information on EDC fitting. The resulting electronic temperature is shown as red dots in Fig. 3c, which was fitted by a convolution between a

Gaussian pulse and a single exponential decay as shown by red line. From the fitting curve, we can extract a decay time of 0.26 ps. It should be noted that the surface states in topological insulators have a longer lifetime^{46–50} compared to the surface state of ZrSiS. Further, the ultrafast dynamics of the surface states in topological insulators have a delayed response compared to the bulk states which is strikingly different in ZrSiS as the surface state carriers decay quite faster than the bulk states. In a topological insulator, the high-lying bulk states rapidly decay to lower energy levels via inter- and intraband phonon mediated scattering processes which acts as an electron reservoir providing a constant supply of carriers to the surface states thus making the surface states considerably long-

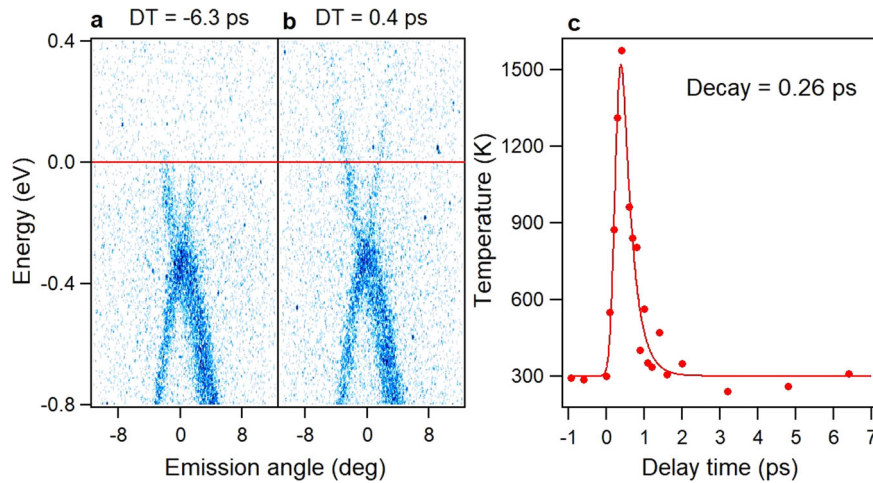


Fig. 3 Time-resolved angle-resolved photoemission spectroscopy measurements of the Dirac-like surface states. Experimental band dispersion measured along the $X-M$ direction at delay times of **a** -6.3 ps and **b** 0.4 ps. **c** The transient electronic temperature as a function of the time delay (red dots) and the corresponding fitting curve (red line). The fitting function is the convolution between a Gaussian pulse and a single exponential decay.

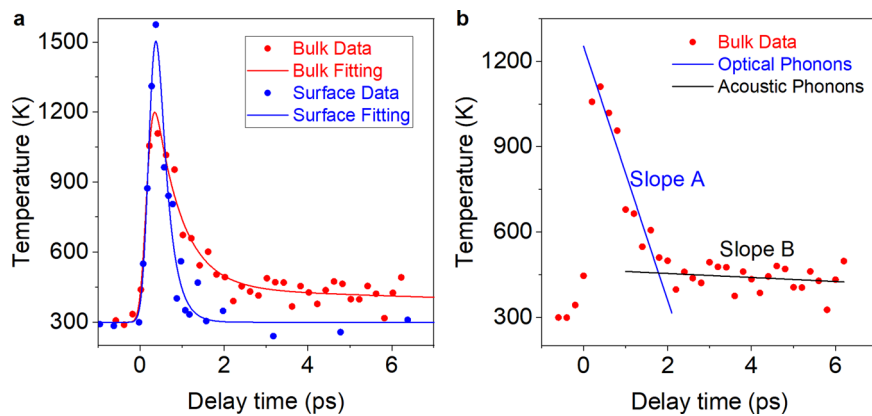


Fig. 4 Theoretical modeling of experimentally obtained data. **a** Comparison between the transient electronic temperature of the nodal-line bulk and the surface states. The measured temperature data are shown as dots, with the convolution fitting shown as lines. The decay time of the nodal-line bulk state is found to be longer than the surface state. **b** The measured bulk temperatures are shown as red dots. The blue and black lines, which are obtained from our theory, represent the optical and acoustic phonons, respectively.

lived^{46,47}. In the present case the bulk-states are short-lived and so cannot supply electrons for a long time, which may be one of the reasons for the short-lived surface states in ZrSiS compared to topological insulators. However, further detailed studies need to be performed to decipher the fast relaxation dynamics of the surface states of ZrSiS compared to its bulk state.

Theoretical interpretation of relaxation dynamics. In order to compare the ultrafast relaxation dynamics between the nodal-line bulk state and the Dirac-like surface state, we plotted the transient electronic temperature as a function of the delay time in Fig. 4a. We observe that the temperature increases rapidly for both the bulk and the surface states, soon after the photoexcitation of the electrons due to the pump pulse. Interestingly, the relaxation dynamics in the cooling process is quite different. The relaxation time for the Dirac-like surface state is around ~ 0.26 ps, which is equivalent or smaller than the time resolution of our set-up. We can attribute this to the electron–electron interaction process¹⁴. For the nodal-line bulk state, there are two prominent features. One is the fast relaxation decay with a time scale of ~ 0.6 ps, the other is a persistent state, with decay constant of around ~ 20 ps.

To understand the underlying physics of the unique features of the transient nodal-line bulk state, we compute the temperature relaxation due to optical and (longitudinal) acoustic phonons using a two-band model of a nodal-line semimetal. The relaxation model is

$$\frac{d\mathcal{E}}{dt} = -\frac{1}{V} \sum_{nk} \epsilon_{nk} \frac{df_{nk}}{dt}, \quad (1)$$

where the energy

$$\mathcal{E} = \frac{1}{V} \sum_{nk} \epsilon_{nk} f_{nk}, \quad (2)$$

is a function of a time-dependent temperature and chemical potential $\mathcal{E}(t) = \mathcal{E}(\mu(t), T_e(t))$. The collision integral for phonons is

$$\frac{df_{nk}}{dt} = \sum_{mp} [f_{nk}(1-f_{mp})W_{nk,mp} - (nk \leftrightarrow mp)], \quad (3)$$

$$W_{nk,mp} = \frac{2\pi}{\hbar} \sum_{\mathbf{q}} M_{\mathbf{q}} [(N_{\mathbf{L}} + 1) \delta_{\mathbf{k}, \mathbf{p}+\mathbf{q}} \delta(\epsilon_{nk} - \epsilon_{mp} - \hbar\omega_{\mathbf{q}}) + N_{\mathbf{L}} \delta_{\mathbf{k}, \mathbf{p}-\mathbf{q}} \delta(\epsilon_{nk} - \epsilon_{mp} + \hbar\omega_{\mathbf{q}})], \quad (4)$$

where $M_{\mathbf{q}} = \hbar^2 D^2 q^2 (1 + s_{nm} \cos \theta) / 4\rho V \hbar \omega_{\mathbf{q}}$ is the amplitude of phonon–electron scattering, \mathbf{q} is the phonon momentum, $\omega_{\mathbf{q}}$ is the phonon dispersion relation, D is the deformation potential of acoustic phonons, ρ the ion mass density, V is the volume, θ the angle between \mathbf{k} and \mathbf{p} , and $s_{nm} = 1$ for intraband and -1 for interband scattering. To obtain an analytical expression we evaluate the collision integral to lowest order in the small c/v limit where c is the sound speed.

In the regime applicable to our experiment, we find a linear temperature relaxation due to optical phonons. We have fitted the experimental data in Fig. 4b with the equation

$$k_B T_e = k_B T_0 - \hbar \omega_0 \gamma_o t, \quad (5)$$

obtaining the slope A . Here ω_0 , T_e , T_0 and T_L are the optical phonon energy, electron temperature, initial electron temperature (1200 K), lattice temperature, respectively and $\gamma_o = 3g^2 Q \omega_0^2 (1/6 + 2\bar{\mu}^3/3) / \pi^2 v^2 \hbar \mu$ where g = electron–optical phonon coupling, μ is the chemical potential (see Supplementary Note 3 for more details). The slope B in Fig. 4b is fitted due to relaxation associated with the acoustic phonons using the equation

$$k_B T_e = k_B T_0 - \gamma_a t \quad (6)$$

where $\gamma_a = 3D^2 Q^3 \epsilon_F / 4\pi^2 \rho \hbar v^2$ (see Supplementary Note 3 for more details). Using the parameters as shown in Supplementary Table 1, the slope A and slope B as shown by solid lines in Fig. 4b obtained from theoretical fits are -439.6 and -7.07 K/ps, respectively. This is in good agreement with the experimental fit for both slope A and slope B as -446.44 and -7 K/ps, respectively. This suggests that when the electronic temperature is high, optical phonon scattering dominates and at low temperature acoustic phonon dominate. When the Fermi energy is close to the nodal-line, relaxation due to acoustic phonon is strongly suppressed for all the temperatures above the lattice temperatures. This is because the nodal ring constrains the acoustic phonons to a very narrow region of momentum space.

Conclusion

In conclusion, we have performed XUV-based tr-ARPES measurements on a topological nodal-line semimetal ZrSiS. The detailed analysis of the transient ARPES spectra as a function of the time delay suggests the ultrafast relaxation of the hot electrons in the nodal-line bulk state is much longer than the surface states. In addition to this, for the nodal-line bulk states, we find that at high electron temperatures the optical–phonon relaxation time scale is much shorter than the time scale corresponding to acoustic phonons and may be evidence of a more general mechanism in TNSMs. Our results provide first insights into electron cooling process for the nodal-line bulk state via energy exchange with the lattice.

Methods

Single crystal growth. High-quality single crystals of ZrSiS were grown by the vapor transport method. The details of the preparation method are described elsewhere^{38–40}. The grown samples were characterized by X-ray diffraction and transport measurements. The samples were flat and shiny which were suitable for ARPES measurements. The chemical composition was verified by an energy-dispersive X-ray analysis using a FEI scanning electron microscope equipped with an energy-dispersive X-ray analysis Genesis XM4 spectrometer. The crystal structure was examined at room temperature on a Kuma-Diffraction KM4 four-circle X-ray diffractometer equipped with a CCD camera using Cu K α radiation. The experiment confirmed the tetragonal crystal structure which is in good agreement with a previous report⁴⁰.

Angle-resolved photoemission spectroscopy. The ultrashort-laser based ARPES measurements were performed at the Laboratory for Advanced Spectroscopic Characterization of Quantum Materials. The samples were cleaved in the ultra-high vacuum ($\sim 3 \times 10^{-10}$ torr) at a temperature of 300 K, and band structures were

measured with Scienta R3000 analyzer at room temperature. The momentum and energy resolution were better than 0.2° and 30 meV, respectively. Synchrotron-based ARPES measurements were carried out at the SIS-HRPES end station of the Swiss Light Source with a Scienta R4000 hemispherical electron analyzer. The energy and momentum resolution were set to be better than 20 meV and 0.2° , respectively for the synchrotron measurements.

Time-resolved angle resolved photoemission spectroscopy. The relaxation dynamics of the nodal-line bulk state and the surface state of ZrSiS was studied using Yb:KGW amplifier-based tr-ARPES set-up with an ultrashort XUV source of 21.8 eV. The high photon energy of 21.8 eV is very important for accessing a relatively large momentum area since the Dirac-like surface state is near the edge of the Brillouin zone. The pump fluence for all the measurements is kept approximately at 760 $\mu\text{J}/\text{cm}^2$. The energy of the pump pulse is 1.2 eV (1025 nm) and the average power is 20 W for repetition rates between 50 and 200 kHz. A schematic illustration of the geometry of our tr-ARPES experiment is shown in Fig. 1a and the details of the experimental set-up is given in ref. ⁵¹.

Data availability

The data supporting the findings of this study are available within the paper, and other findings of this study are available from the corresponding author upon reasonable request.

Received: 28 December 2021; Accepted: 22 July 2022;

Published online: 10 August 2022

References

- Hasan, M. Z., Xu, S.-Y. & Neupane, M. In *Topological Insulators: Fundamentals and Perspectives* (eds. Ortman, F. Roche, S. & Valenzuela, S. O.) Ch. 4 (John Wiley & Sons, 2015).
- Hasan, M. Z. & Kane, C. L. Colloquium: Topological insulators. *Rev. Mod. Phys.* **82**, 3045 (2010).
- Qi, X.-L. & Zhang, S.-C. Topological insulators and superconductors. *Rev. Mod. Phys.* **83**, 1057 (2011).
- Bansil, A., Lin, H. & Das, T. Colloquium: Topological band theory. *Rev. Mod. Phys.* **88**, 021004 (2016).
- Weng, H., Dai, X. & Fang, Z. Topological semimetals predicted from first-principles calculations. *J. Phys. Condens. Matter* **28**, 303001 (2016).
- Hasan, M. Z., Xu, S.-Y., Belopolski, I. & Huang, S.-M. Discovery of Weyl fermion semimetals and topological Fermi arc states. *Annu. Rev. Condens. Matter Phys.* **8**, 289 (2017).
- Armitage, N. P., Mele, E. J. & Vishwanath, A. Weyl and Dirac semimetals in three-dimensional solids. *Rev. Mod. Phys.* **90**, 015001 (2018).
- Burkov, A. A., Hook, M. D. & Balents, L. Topological nodal semimetals. *Phys. Rev. B* **84**, 235126 (2011).
- Neupane, M. et al. Observation of topological nodal fermion semimetal phase in ZrSiS. *Phys. Rev. B* **93**, 201104 (2016).
- Schoop, L. M. et al. Dirac cone protected by non-symmorphic symmetry and three-dimensional Dirac line node in ZrSiS. *Nat. Commun.* **7**, 1–7 (2016).
- Klemenz, S., Lei, S. & Schoop, L. M. Topological semimetals in square-set materials. *Annu. Rev. Mater. Res.* **49**, 185 (2019).
- Fang, C., Weng, H., Dai, X. & Fang, Z. Topological nodal line semimetals. *Chin. Phys. B* **25**, 117106 (2016).
- Chiu, C.-K., Teo, J. C. Y., Schnyder, A. P. & Ryu, S. Classification of topological quantum matter with symmetries. *Rev. Mod. Phys.* **88**, 035005 (2016).
- Gatti, G. et al. Light-induced renormalization of the Dirac quasiparticles in the nodal-line semimetal ZrSiSe. *Phys. Rev. Lett.* **125**, 076401 (2020).
- Kim, Y., Wieder, B. J., Kane, C. L. & Rappe, A. M. Dirac line nodes in inversion-symmetry crystals. *Phys. Rev. Lett.* **115**, 036809 (2015).
- Yu, R., Fang, Z., Dai, X. & Weng, H. M. Topological nodal line semimetals predicted from first-principles calculations. *Front. Phys.* **12**, 127202 (2017).
- Xu, Q. N., Yu, R., Fang, Z., Dai, X. & Weng, H. M. Topological nodal line semimetals in the CaP₃ family of materials. *Phys. Rev. B* **95**, 045136 (2017).
- Yang, S. Y. et al. Symmetry demanded topological nodal-line materials. *Adv. Phys. X* **3**, 1414631 (2018).
- Chan, Y.-H., Chiu, C.-K., Chou, M. Y. & Schnyder, A. P. Ca₃P₂ and other topological semimetals with line nodes and drumhead surface states. *Phys. Rev. B* **93**, 205132 (2016).
- Bian, G. et al. Topological nodal-line fermions in spin-orbit metal PbTaSe₂. *Nat. Commun.* **7**, 10556 (2016).
- Belopolski, I. et al. Discovery of topological Weyl fermion lines and drumhead surface states in a room temperature magnet. *Science* **365**, 1278 (2019).

22. Hosen, M. M. et al. Experimental observation of drumhead surface states in SrAs₃. *Sci. Rep.* **10**, 2776 (2020).
23. Lou, R. et al. Experimental observation of bulk nodal lines and electronic surface states in ZrB₂. *npj Quantum Mater.* **3**, 43 (2018).
24. Sims, C. M. et al. Termination dependent topological surface states in nodal-loop semimetal HfP₂. *Phys. Rev. Mater.* **4**, 054201 (2020).
25. Kirby, R. J. et al. Transient drude response dominates near-infrared pump-probe reflectivity in nodal-line semimetals ZrSiS and ZrSiSe. *J. Phys. Chem. Lett.* **11**, 6105–6111 (2020).
26. Liu, J. & Balents, L. Correlation effects and quantum oscillations in topological nodal-loop semimetals. *Phys. Rev. B* **95**, 075426 (2017).
27. Rudenko, A. N. & Yuan, S. Electron-phonon interaction and zero-field charge carrier transport in the nodal-line semimetal ZrSiS. *Phys. Rev. B* **101**, 115127 (2020).
28. Topp, A. et al. Non-symmorphic band degeneracy at the Fermi level in ZrSiTe. *N. J. Phys.* **18**, 125014 (2016).
29. Hu, J. et al. Evidence of topological nodal-line fermions in ZrSiSe and ZrSiTe. *Phys. Rev. Lett.* **117**, 016602 (2016).
30. Hosen, M. M. et al. Tunability of the topological nodal-line semimetal phase in ZrSiX-type materials (X = S, Se, Te). *Phys. Rev. B* **95**, 161101 (2017).
31. Chen, C. et al. Dirac line nodes and effect of spin-orbit coupling in the nonsymmorphic critical semimetals MSi(M = Hf, Zr). *Phys. Rev. B* **95**, 125126 (2017).
32. Lou, R. et al. Emergence of topological bands on the surface of ZrSnTe crystal. *Phys. Rev. B* **93**, 241104 (2016).
33. Hu, J. et al. Quantum oscillation evidence for a topological semimetal phase in ZrSnTe. *Phys. Rev. B* **97**, 155101 (2018).
34. Zhang, J. et al. Transport evidence of 3D topological nodal-line semimetal phase in ZrSiS. *Front. Phys.* **13**, 137201 (2017).
35. Hosen, M. M. et al. Observation of gapless Dirac surface states in ZrGeTe. *Phys. Rev. B* **97**, 121103 (2018).
36. Yen, Y. et al. Dirac nodal line and Rashba spin-split surface states in nonsymmorphic ZrGeTe. *N. J. Phys.* **23**, 103019 (2021).
37. Fu, B.-B. et al. Dirac nodal surfaces and nodal lines in ZrSiS. *Sci. Adv.* **5**, eaau6459 (2019).
38. Wang, C. & Hughbanks, T. Main group element size and substitution effects on the structural dimensionality of zirconium tellurides of the ZrSiS type. *Inorg. Chem.* **34**, 5524–5529 (1995).
39. Singha, R., Pariari, A. K., Satpati, B. & Mandal, P. Large nonsaturating magnetoresistance and signature of nondegenerate Dirac nodes in ZrSiS. *Proc. Natl Acad. Sci. USA* **114**, 2468–2473 (2017).
40. Sankar, R. et al. Crystal growth of Dirac semimetal ZrSiS with high magnetoresistance and mobility. *Sci. Rep.* **7**, 40603 (2017).
41. Su, C.-C. et al. Surface termination dependent quasiparticle scattering interference and magneto-transport study on ZrSiS. *N. J. Phys.* **20**, 103025 (2018).
42. Schilling, M. B., Schoop, L. M., Lotsch, B. V., Dressel, M. & Pronin, A. V. Flat optical conductivity in ZrSiS due to two-dimensional Dirac bands. *Phys. Rev. Lett.* **119**, 187401 (2017).
43. Matusiak, M., Cooper, J. & Kaczorowski, D. Thermoelectric quantum oscillations in ZrSiS. *Nat. Commun.* **8**, 15219 (2017).
44. Weber, C. P. et al. Directly photoexcited Dirac and Weyl fermions in ZrSiS and NbAs. *Appl. Phys. Lett.* **113**, 221906 (2018).
45. Weber, C. P. Ultrafast investigation and control of Dirac and Weyl semimetals. *J. Appl. Phys.* **129**, 070901 (2021).
46. Sobota, J. A. et al. Ultrafast optical excitation of a persistent surface-state population in the topological insulator Bi₂Se₃. *Phys. Rev. Lett.* **108**, 117403 (2012).
47. Hajlaoui, M. et al. Ultrafast surface carrier dynamics in the topological insulator Bi₂Te₃. *Nano Lett.* **12**, 3532–3536 (2012).
48. Wang, Y. et al. Measurement of intrinsic Dirac fermion cooling on the surface of the topological insulator Bi₂Se₃ using time-resolved and angle-resolved photoemission spectroscopy. *Phys. Rev. Lett.* **109**, 127401 (2012).
49. Crepaldi, A. et al. Ultrafast photodoping and effective Fermi-Dirac distribution of the Dirac particles in Bi₂Se₃. *Phys. Rev. B* **86**, 205133 (2012).
50. Neupane, M. et al. Gigantic surface lifetime of an intrinsic topological insulator. *Phys. Rev. Lett.* **115**, 116801 (2015).
51. Liu, Y. et al. Extreme ultraviolet time-and angle-resolved photoemission setup with 21.5 meV resolution using high-order harmonic generation from a turn-key Yb:KGW amplifier. *Rev. Sci. Instrum.* **91**, 013102 (2020).

Acknowledgements

M.N. acknowledges support from the Air Force Office of Scientific Research under Award No. FA9550-17-1-0415 and the Air Force Office of Scientific Research MURI (FA9550-20-1-0322). B.M.F. acknowledges support from NSF grant DMR-2015639 and DOE-NERSC under contract DE-AC02-05CH11231. M.C. acknowledges support from the Air Force Office of Scientific Research under Award Numbers FA9550-16-1-0149 and FA9550-20-1-0284.

Author contributions

M.N. conceived the project; D.K. synthesized the samples and performed the electrical transport characterizations. Y.L. and G.D. performed the measurements with the help of A.P.S., J.E.B., F.K., S.R., M.C., and M.N.; Y.L. and M.N. performed the data analysis and figure planning. B.M.F. carried out the theoretical analysis in consultation with Y.L., A.P.S., and M.N.; M.C. supervised pump-probe experiments. Y.L. and M.N. wrote the manuscript with input from all authors. M.N. was responsible for the overall research direction, planning, and integration among different research units. All authors discussed the results, interpretation and conclusion.

Competing interests

The authors declare no competing interests.

Additional information

Supplementary information The online version contains supplementary material available at <https://doi.org/10.1038/s42005-022-00980-6>.

Correspondence and requests for materials should be addressed to Benjamin M. Fregoso or Madhab Neupane.

Peer review information *Communications Physics* thanks the anonymous reviewers for their contribution to the peer review of this work.

Reprints and permission information is available at <http://www.nature.com/reprints>

Publisher's note Springer Nature remains neutral with regard to jurisdictional claims in published maps and institutional affiliations.



Open Access This article is licensed under a Creative Commons Attribution 4.0 International License, which permits use, sharing, adaptation, distribution and reproduction in any medium or format, as long as you give appropriate credit to the original author(s) and the source, provide a link to the Creative Commons license, and indicate if changes were made. The images or other third party material in this article are included in the article's Creative Commons license, unless indicated otherwise in a credit line to the material. If material is not included in the article's Creative Commons license and your intended use is not permitted by statutory regulation or exceeds the permitted use, you will need to obtain permission directly from the copyright holder. To view a copy of this license, visit <http://creativecommons.org/licenses/by/4.0/>.

© The Author(s) 2022